

RESEARCH ARTICLE | MARCH 27 2024

Reciprocity relations in a biologically inspired nanomagnonic system with dipolar coupling

Special Collection: [Magnonics](#)

Benjamin W. Zingsem  ; Thomas Feggeler  ; Detlef Spoddig  ; Ralf Meckenstock  ; Michael Farle  ; Michael Winklhofer  



Appl. Phys. Lett. 124, 132405 (2024)
<https://doi.org/10.1063/5.0195215>



Nanotechnology & Materials Science


Optics & Photonics

Impedance Analysis

Scanning Probe Microscopy


Sensors

Failure Analysis & Semiconductors



Unlock the Full Spectrum.
From DC to 8.5 GHz.
Your Application. Measured.

[Find out more](#)



Reciprocity relations in a biologically inspired nanomagnonic system with dipolar coupling

Cite as: Appl. Phys. Lett. **124**, 132405 (2024); doi: [10.1063/5.0195215](https://doi.org/10.1063/5.0195215)

Submitted: 31 December 2023 · Accepted: 14 March 2024 ·

Published Online: 27 March 2024



View Online



Export Citation



CrossMark

Benjamin W. Zingsem,¹  Thomas Feggeler,^{2,3}  Detlef Spoddig,⁴  Ralf Meckenstock,⁴  Michael Farle,⁴ 
and Michael Winklhofer^{5,6,a)} 

AFFILIATIONS

¹Ernst-Ruska Centre for Microscopy and Spectroscopy with Electrons, Forschungszentrum Jülich, 52428 Jülich, Germany

²Department of Physics, University of California, Berkeley, Berkeley California 94720, USA

³Advanced Light Source, Lawrence Berkeley National Laboratory, Berkeley California 94720, USA

⁴Faculty of Physics and Center for Nanointegration Duisburg-Essen (CENIDE), University of Duisburg-Essen, 47048 Duisburg, Germany

⁵Institut für Biologie und Umweltwissenschaften, Carl von Ossietzky Universität Oldenburg, 26129 Oldenburg, Germany

⁶Forschungszentrum Neurosensorik, Carl von Ossietzky Universität Oldenburg, 26111 Oldenburg, Germany

Note: This paper is part of the APL Special Collection on Magnonics.

^{a)}Author to whom correspondence should be addressed: michael.winklhofer@uol.de

ABSTRACT

Magnetosome chains in magnetotactic bacteria present ideal nanomagnonic model systems for studying collective resonance modes of dipolar-coupled single domain particles in relation to their spatial arrangement. Using microresonator-based ferromagnetic resonance (FMR) spectroscopy, electron microscopy, and micromagnetic modeling, we here provide insights into the complex magnonic activity within a single magnetosome chain. While the angular dependence of its FMR spectrum is dominated by twofold symmetry features due to the uniaxial anisotropy of linear chain segments, we also observed an unexpected behavior such as interrupted lines and flat bands due to the intricate geometrical details of this particular chain, such as a cross-like structural anomaly where a pair of particles is oriented perpendicular to the main axis of the chain and thus breaks the prevailing axial dipolar coupling symmetry. Such a cross junction formed by four particles exhibits interesting magnonic network properties. Notably, we observe reciprocity in the sense that the spectral response of one particle to an excitation of another one is identical to the response of the latter given an excitation of the former. Furthermore, we have identified that magnonic coupling between A and B can be facilitated via a dark state, as in magnonic stimulated Raman adiabatic passage, and that this dark-state coupling can be made non-reciprocal between A and B by breaking the symmetry of the spatial arrangement of the four particles.

Published under an exclusive license by AIP Publishing. <https://doi.org/10.1063/5.0195215>

Magnetotactic bacteria produce intracellular membrane-enclosed magnetic particles called magnetosomes and do so in a strictly biologically controlled way, yielding single-domain magnetic particles with consistent shapes and sizes. Therefore, they present a rich platform for multidisciplinary research,^{1–4} opening avenues for advanced material science^{3,5,6} and electron^{1,7–11} and x-ray^{12–16} microscopy studies. The magnetosomes are arranged in the form of chains, with the magnetic polarity of each particle summing up coherently to yield the maximum possible cellular magnetic dipole moment, instrumental in guiding the whole cell along geomagnetic field lines, referred to as magnetotaxis.¹⁷ Intriguingly, these chains of dipolar coupled particles exhibit a richness of magnonic behaviors, which invites concepts for spin-wave devices operating at the nanoscale.^{18,19}

In this study, we focus on the magnonic properties of a single magnetosome chain, measured at room temperature with angular-dependent ferromagnetic resonance (FMR) spectroscopy using a microresonator^{24,25} operated at 8.87 GHz. The precision of these measurements allows for the identification of both individual particle modes and collective resonance modes, a phenomenon that remains underexplored in existing literature, due to the limited sensitivity of conventional broadband and resonator based FMR. Using the chain geometry reconstructed from electron microscopy, we micromagnetically simulate the magnonic behavior to understand the magnonic activity within this biological structure. It turns out that the most fascinating behavior is generated by a cross-like structural anomaly in the chain, where a pair of magnetite nanoparticles is arranged

perpendicular to the chain axis. Simulating excitation-response matrices for four particles in a cross-like arrangement, we find interesting reciprocity relations, dark state coupling, and magnonic stimulated Raman adiabatic passage (StiRAP), which was described recently in magnonic wave guides.²⁰

For our experiment, we used cells of magnetotactic bacteria commercially available in pure culture (*Magnetospirillum gryphiswaldense*²⁶ strain MSR-1). Cells were transferred into a HEPES buffer, suctioned into a pipette, and dropped on a TEM carbon-coated copper grid. The grid was transferred into an FEI Helios NanoLabTM 600 dual-beam FIB/SEM system to mill out a patch of the carbon film featuring an isolated single cell. The excised carbon film with the cell was placed inside the loop of a μ -resonator,²⁵ thereby ascertaining that the μ -resonator was loaded with a single cell containing a single magnetosome chain [Fig. 1(a)].

The microresonator-based angular dependent ferromagnetic resonance (FMR) measurements were performed at 8.87 GHz and 50 mW input power using a custom-built continuous wave X-band FMR spectrometer consisting of a rotatable electromagnet, a Hall probe, and a Varian E-102 microwave bridge. The setup measures the microwave power reflected off the μ -resonator with a microwave detector integrated into the microwave bridge. For improved FMR sensitivity, the detected voltage is recorded by a Stanford Research SR 830 lock-in amplifier using as reference the signal of an incorporated field modulation at 123.45 Hz and 0.5 mT amplitude, which overlays the static DC magnetic field. The DC field was swept from 200 to 400 mT in steps of 0.5 mT with the resonator's in-plane orientation altered in a range of 180 degrees by 1-degree steps.

Micromagnetic simulations were performed using the GPU-accelerated simulation software Mumax3.^{22,23} The overall FMR spectrum of the magnetosome chain was simulated using a sinc-pulse excitation¹⁹ to enhance performance. Additionally, we validated our results with a continuous wave (CW)-type simulation (see the supplementary material for simulation details). Both simulations reveal the magnonic ground state spectrum ($k = 0$), i.e., the ferromagnetic resonance spectrum of the particle chain. The key difference is that in the sinc-pulse excitations mode, scattering cannot be distinguished, as all modes are excited equally with a broad spectral pulse. In the CW excitation, on the other hand, individual modes are excited by applying continuous wave signals at fixed frequencies. In both excitation modes, the overall angular dependency of the simulated FMR spectra is identical, along with the typical features of multiple modes and mode interruptions.

Additional simulations were performed on a junction composed of four particles; a highly symmetric representation of the central area of the magnetosome chain [highlighted in red in Fig. 1(a)]. We focused on the spectral response S_{ij} of particle i to a selective sinc-pulse excitation of particle j ($i, j = 1, \dots, 4$). Furthermore, we modeled the responses of this entire ensemble ($i = 0$) to excitations of individual particles ($j = 1, \dots, 4$) and, vice versa, the responses of individual particles ($i = 1, \dots, 4$) to excitations of the entire ensemble ($j = 0$). The complete S_{ij} matrix thus has a 5×5 structure. Identical simulations were performed on a less symmetric representation of this junction.

The sample [Fig. 1(a)] from which we recorded angular dependent FMR spectra [Fig. 1(b)] was a magnetosome chain composed of ca. 20–30 crystals of magnetite (ca. 25 nm diameter), spaced apart by about 5 nm, with a total chain length of approximately 1 μ m.

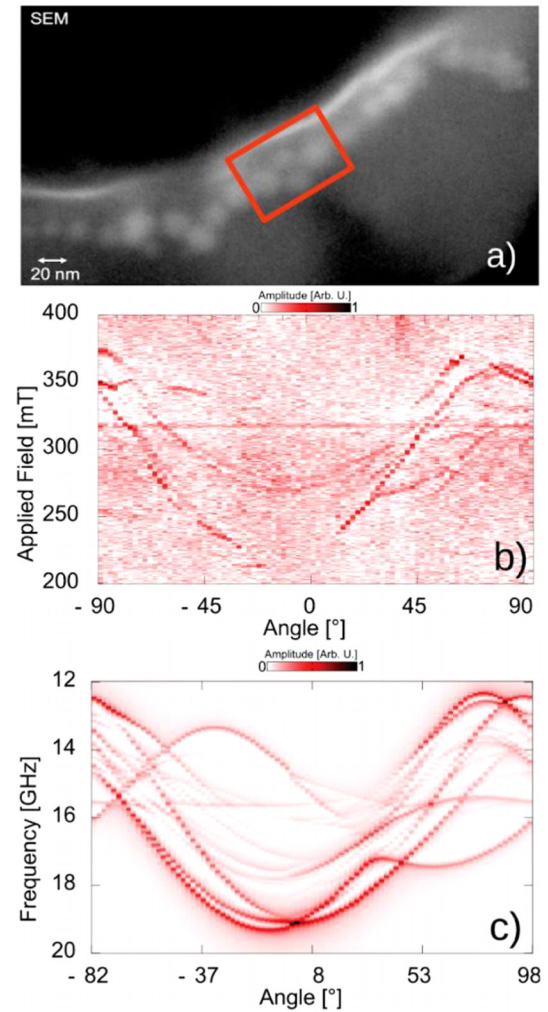


FIG. 1. Sample and FMR Spectra: (a) SEM micrograph of the magnetosome chain still encapsulated by the bacteria cell, as used in the FMR experiments. The rectangle highlights the four-particle junction in the center of the chain. (b) FMR spectrum of the chain, recorded at 8.87 GHz. The gray dashed arrow (bottom right) shows the direction corresponding to 0° , relative to the chain. (c) Frequency-dependent FMR spectrum obtained from sinc-type micromagnetic simulations at an applied field of 600 mT. The field was rotated clockwise. The black arrow to the right shows the direction corresponding to 0° . (d) For each particle in the model, a color was assigned (compare the model to the right). At each resonance detected in (c), a point was placed with the color corresponding to that particle in the chain, contributing to this resonance with the highest amplitude.

The FMR lines are very narrow [ca. 1 mT, see Fig. S1(c)], indicating exceptionally small damping compared to synthetic magnetite thin films deposited on substrates.²⁷ The simulated FMR spectrum [Fig. 1(c)] of the chain model (depicted at the bottom of Fig. 1) allows us to identify the origin of some features in the experimental spectrum. For this purpose, we have colored the spectral lines from the simulation according to the particle that contributes most to it [Fig. 1(d)]. It can be seen that the major axis of the chain produces the line with the strongest intensity and largest anisotropy, following a twofold

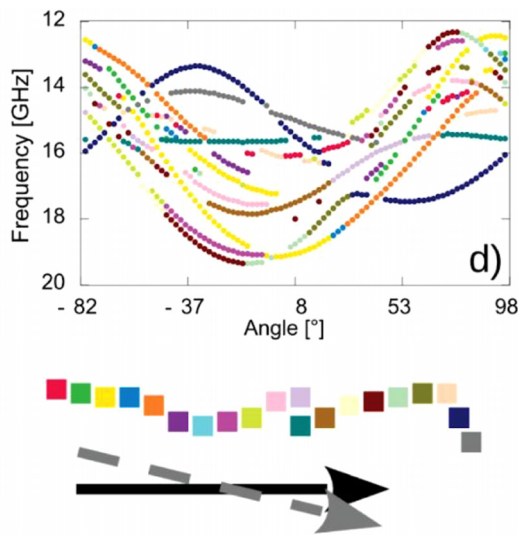


FIG. 1. (Continued.)

symmetry induced by the overall shape anisotropy of the chain. In contrast, the short segment—bent away from the main axis at the upper end—gives rise to the resonance line [shown in the dark blue in Fig. 1(d)], which is offset by ca. 60° from the main line but still has twofold symmetry, albeit with a weaker anisotropy due to the comparatively short length of that segment.

From the micromagnetic simulations, we find that the particle size is sufficiently small to suppress edge modes.^{19,21} Each particle behaves as a single oscillator, responding only with a $k = 0$ mode (uniform oscillation). At the same time, the entire chain exhibits modes of $k \neq 0$, where neighboring oscillators respond at a different phase, minimizing the dipolar energy of the coupled system and effectively forming a standing wave envelope across multiple particles.

While the overall symmetry of the spectrum in Figs. 1(b) and 1(d) displays a twofold symmetry, intricate details of the chain geometry give rise to interesting phenomena. In particular, individual resonance lines are not only offset to the overall twofold symmetry but bear completely different angular dependencies. This includes distortions of the resonance's angular-dependent symmetry, avoided crossings, and spectral interruptions, which were previously¹⁹ identified to be due to the commensurability of the magnonic ground states in different segments. Hence, to understand the features of the spectrum in detail, the exact geometric composition of the chain has to be considered. As a first step toward a full understanding of this complex magnonic coupling, we focus here on the cross-like substructure near the center of the chain [highlighted in red in Fig. 1(a)], due to a pair of particles oriented perpendicular to the main axis of the chain. This pair breaks the prevailing axial dipolar coupling symmetry. To illustrate the spectral responses to stimuli of different localization, we have computed the four-port S_{ij} matrix of a highly symmetric cross-like junction (Fig. 2), in comparison to a maximally asymmetric junction (Fig. 3) as a more realistic representation of the actual chain geometry.

For the case of the highly symmetric cross-like junction, one can see that a spatially uniform excitation (left column in Fig. 2) produces

two modes (S_{00}), one dominated by the responses of the outer particles (S_{10} and S_{40}), the other one dominated by the response of the inner particles (S_{20} and S_{30}), the latter becoming somewhat attenuated as the field angle approaches the long axis of the junction. Band gaps appear in each spectrum where high energy and low energy modes repel each other because of incompatible spatial mode profiles.^{18,19} When looking at the symmetry properties of the S_{ij} matrix, we find that the spectral characteristics obey reciprocity in the sense that the spectral response S_{ij} of particle $i = \mu$, due to an excitation of particle $j = \nu$, is identical to that of particle $j = \mu$, due to the excitation of particle $i = \nu$, i.e., $S_{ji} = S_{ij}$. This is contrary to the naive assumption that the resonant properties of a particle are solely determined by its local dipolar environment. This view only holds when a given particle responds to an excitation of that same particle (compare the diagonal S_{ii}). If, however, the excitation is mediated via dipolar coupling and through additional particles, then the available modes are filtered, and as a result, reciprocity among the spectra is established.

To confirm that spectral reciprocity is not an artificial property of the highly symmetric geometry of the junction depicted in Fig. 2, but a general aspect of a magnonic circuit based on dipolar coupling, we have performed the same type of simulation on an asymmetric four-particle junction (Fig. 3). Importantly, the reciprocity $S_{ij} = S_{ji}$ is reproduced, despite the broken symmetry. However, the second symmetry plane formed by the antidiagonal of the lower right 4×4 submatrix of the symmetric configuration ($S_{11} = S_{44}$, $S_{22} = S_{33}$, $S_{12} = S_{34}$, etc., in Fig. 2) is absent from the S matrix of the asymmetric configuration (Fig. 3), and therefore the twofold rotation symmetry of the submatrix disappears, too. Likewise, the mirror symmetries apparent in Fig. 2 [$S_{13} = \check{S}_{12}$, $S_{31} = \check{S}_{21}$, $S_{24} = \check{S}_{34}$, $S_{42} = \check{S}_{43}$, with $\check{S}(\varphi) = S(\pi - \varphi)$] are no longer present in the asymmetric configuration (Fig. 3).

To test if reciprocity $S_{ij} = S_{ji}$ generally holds in a dipolarly coupled system, we next included the cubic magnetocrystalline anisotropy energy (MAE) term, which we deliberately neglected thus far. To break the symmetry maximally, we varied the orientation of the cubic $\langle 100 \rangle$ axes system randomly from one particle to the next (“random MAE”). As a control, we oriented the $\langle 100 \rangle$ axes always parallel to the surface normals of the cube-shaped particles (“uniform MAE”). In Figs. S3–S6 of the supplementary material, one can clearly see that the addition of MAE produces different spectra compared to their MAE-free counterparts in Figs. 2 and 3. The pronounced effect of MAE on the spectra of the junction can be explained by its compact geometry, having a much less pronounced shape anisotropy compared to a magnetosome chain (where shape anisotropy dominates over MAE energy). Most importantly though, the coupling matrices always are symmetric about the main diagonal and, thus, reciprocity $S_{ij} = S_{ji}$ is retained, even in the case of random MAE (Figs. S3 and S4). The only change observed concerns the symmetry about the antidiagonal of the matrix for the symmetric junction (compare Fig. 2 with Fig. S3), which is broken in the case of random MAE (Fig. S3). Interestingly, both for the symmetric junction (Fig. S5) and asymmetric junction (Fig. S6), the symmetry properties of the coupling matrix S_{ij} are invariant to the uniform addition of MAE, with S_{ij} of the symmetric junction being symmetric about the antidiagonal (compare Fig. S5 with Fig. 2).

Another interesting feature observed in the symmetric junction can be seen in Fig. 2 (and in Fig. S5) in column $j = 1$ at an applied field angle of 90° , i.e., parallel to the short axis connecting the two inner particles (green arrow in Fig. 2). Here, the left particle can only be

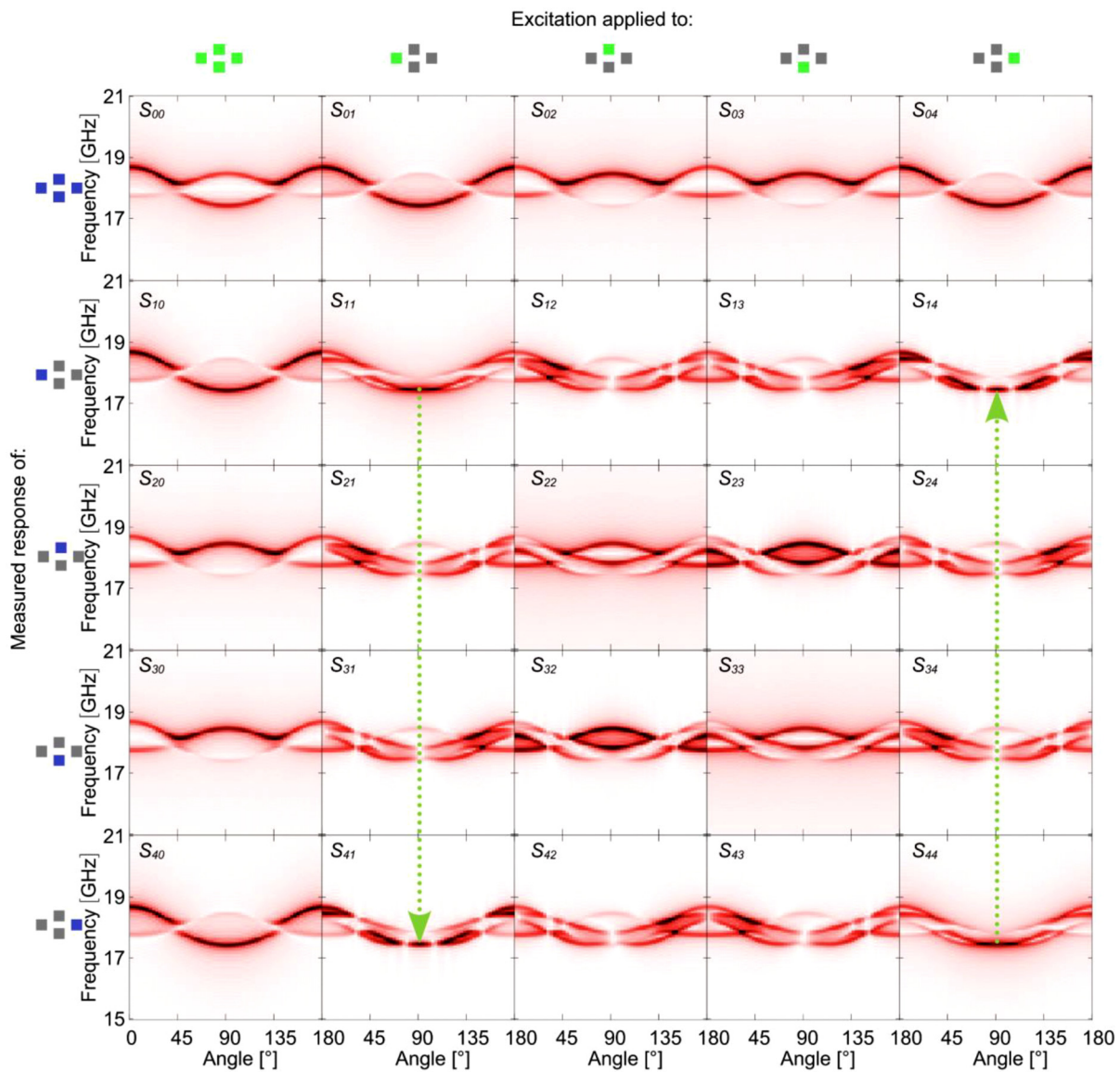


FIG. 2. Simulation of spectral response of the central junction in the chain. S_{00} : angular-dependent frequency components of the magnonic response to a uniform sinc-pulse excitation applied to the entire ensemble. S_{00} : response of the entire particle ensemble. $S_{10} - S_{40}$: individual responses of each of the constituent particles (highlighted in green in the inset). S_{11} : sinc-pulse excitation applied to the leftmost particle. $S_{11} - S_{41}$: individual responses of each of the constituent particles. S_{21} : sinc-pulse excitation applied to the particle located at the top center. $S_{12} - S_{42}$: individual responses of each of the constituent particles. S_{31} : sinc-pulse excitation applied to the particle located at the bottom center. $S_{13} - S_{43}$: individual responses of each of the constituent particles. S_{41} : sinc-pulse excitation applied to the particle on the right. $S_{14} - S_{44}$: individual responses of each of the constituent particles. See Figs. S3 and S5 in the supplementary material for simulations of the symmetric junction with random and uniform MAE, respectively.

excited near 17.5 GHz (low frequency mode of S_{11} at 90° in Fig. 2). In this very spectral range, the angular dependent modes of S_{21} and S_{31} are interrupted, which means each of the two inner particles forms a dark state in the magnonic eigenstate of the system. The state remains unpopulated (dark) in the inner particles, that is, they do not resonate, but nonetheless mediate magnonic coupling between the outer particles. Still, the right particle responds to the excitation of the left particle at the same frequency (S_{41} in Fig. 2). Coupling between the two end magnetic particles across a dark state is similar to the magnonic

StIRAP described in Ref. 20. Regardless of the dark state, the essential role of the inner particles is to mediate strong magnetostatic coupling and thereby facilitate magnonic coupling between the outer particles. This can be seen in a control simulation for just the two outer particles, resulting in single-band spectra without pronounced angular dependence (Fig. S7). Another spectral feature in the angular range about 90° is the presence of a high energy mode at 18.5 GHz (albeit of low spectral amplitude) in S_{21} and S_{31} , which is not present in S_{11} and S_{41} (Fig. 2). Here, energy from the single-particle excitation of the input

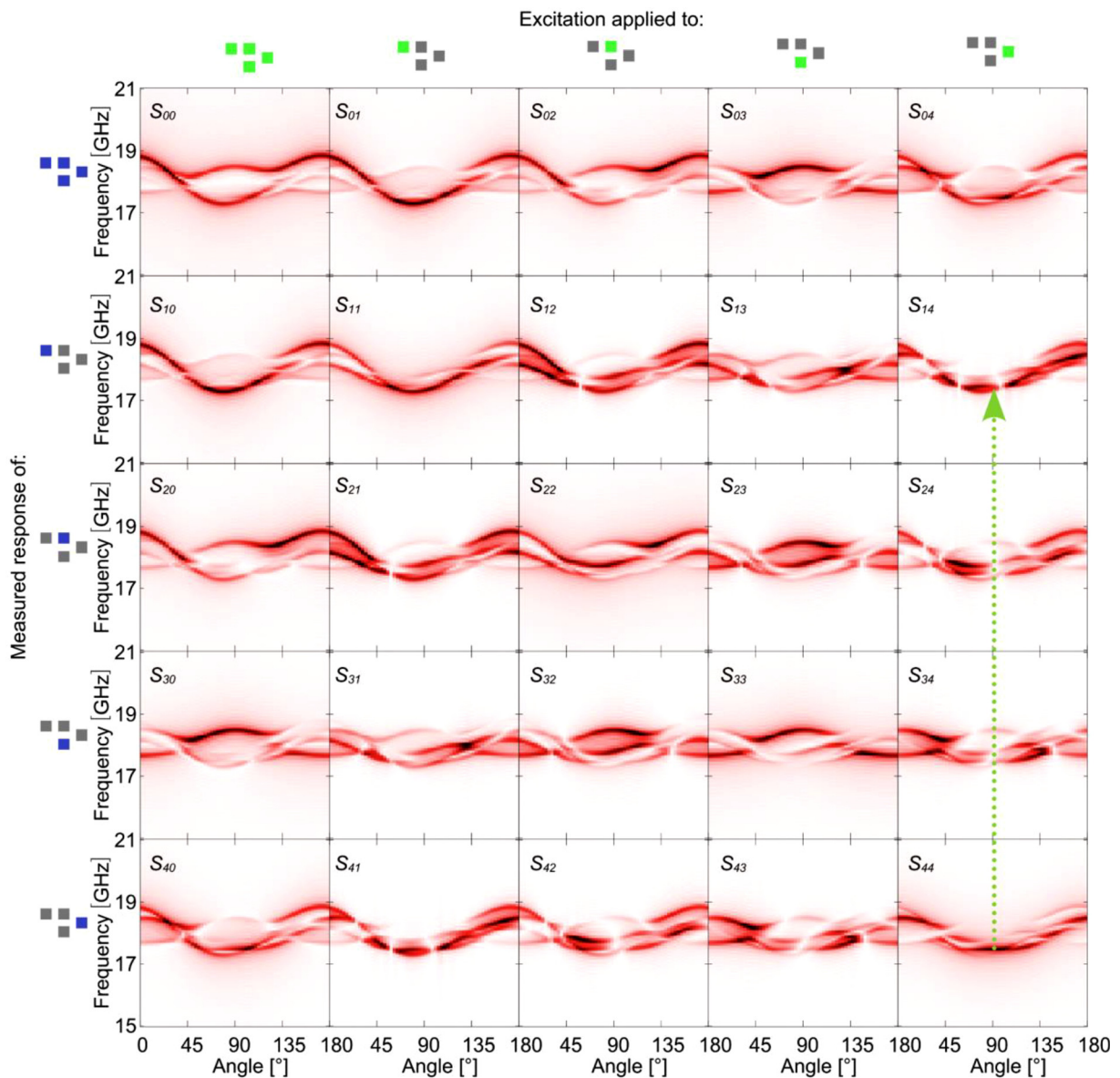


FIG. 3. Effects of geometrical symmetry break on standing wave spectrum: S_{j0} : angular-dependent frequency components of the magnonic response to a uniform sinc-pulse excitation applied to the entire ensemble. S_{00} : response of the entire particle ensemble. $S_{10} - S_{40}$: individual responses of each of the constituent particles (highlighted in green in the inset). S_{11} : sinc-pulse excitation applied to the leftmost particle. $S_{11} - S_{41}$: individual responses of each of the constituent particles. S_{21} : sinc-pulse excitation applied to the particle located at the top center. $S_{12} - S_{42}$: individual responses of each of the constituent particles. S_{22} : sinc-pulse excitation applied to the particle located at the bottom center. $S_{13} - S_{43}$: individual responses of each of the constituent particles. S_{31} : sinc-pulse excitation applied to the particle on the right. $S_{14} - S_{44}$: individual responses of each of the constituent particles. See Figs. S4 and S6 in the supplementary material for simulations of the asymmetric junction with random and uniform MAE, respectively.

particle at a lower frequency of 17.5 GHz is scattered into the higher frequency mode. The mode behavior is observed in S_{12} , except here, a mode at the relevant energy is provided by the input particle as shown in S_{22} . For symmetry reasons, column $j = 4$ (Fig. 2) shares the same features as column $j = 1$, except that now the rightmost particle is being excited. Columns $j = 2, 3$ in Fig. 2 show that energy transfer between the inner particles (S_{32} and S_{23}) at 90° can occur with or

without populating bands in the end particles, depending on whether the mode at higher or lower energy is selected.

In the asymmetric junction, the dark state is still visible as a clear interruption of the angular dependent resonances in the central particles (S_{24} and S_{34} in Fig. 3). However, owing to the broken symmetry ($S_{24} \neq S_{34}$), the spectral gap here is not symmetric, and the dark state is populated to some extent (compare green arrow in Fig. 3).

By comparing column $j = 4$ with $j = 1$ (Fig. 3), it can be seen that the dark-state coupling in the perturbed geometry is non-reciprocal in space. This is due a loss of the twofold rotation symmetry of the 4×4 submatrix, which in the symmetric arrangement ($S_{21} = S_{34}$, $S_{31} = S_{24}$ in Fig. 2) ascertained the spatial reciprocity of the dark-state coupling.

In summary, inspired by the ferromagnetic resonance spectrum of a biogenic assembly of magnetic nanoparticles, we have shown the presence of magnon-circuit reciprocity and magnonic dark state coupling, and how it can be tuned by manipulating the geometry of the arrangement. Our FMR measurements confirm the magnonic response of the system and its symmetry. Using micromagnetic modeling, we reproduce the principal features of the measured FMR spectrum. Further micromagnetic modeling of the four-particle structure at the junction in the center of the magnetosome chain reveals magnonic circuit reciprocity: the spectral response of one particle to an excitation of another one is identical to the response of the latter given an excitation of the former. Furthermore, we have identified that, in such an assembly, magnonic coupling can be facilitated via a dark state, i.e., the lack of magnonic excitation in the part of the system through which the magnonic coupling is mediated between two points. We have also shown that this coupling can be made nonreciprocal, in the sense that an excitation at point A that leads to a magnonic response at point B can couple via a dark state, while the same excitation at point B, leading to the respective response at point A, can be mediated through regular magnonic excitation of the particles between A and B. This last point has been achieved by breaking the spatial (mirror and rotational) symmetry of the geometric arrangement.

See the supplementary material for experimental and numerical methods used as well as results from control simulations.

The authors would like to thank Alexandra Terwey for her help with the experiments. The authors acknowledge the financial support of the German Science Foundation (DFG) in the framework of the Collaborative Research Centres, Transregio 270 (CRC-TRR 270, Project No. 405553726) and CRC-SFB 1372 (Project No. 395940726 to M.W.). T.F. acknowledges support from STROBE: A National Science Foundation Science & Technology Center, under Grant No. DMR-1548924 and Lawrence Berkeley National Laboratory for funding through the LDRD Award: Development of a Continuous Photon Counting Scheme for Time-Resolved Studies. B.Z. acknowledges helpful discussions with Joseph Vimal Vas and technical support by Alexander Clausen and Dieter Weber. The authors acknowledge active support by the Simulation and Data Laboratory electrons & neutrons at the Jülich Supercomputing Centre.

AUTHOR DECLARATIONS

Conflict of Interest

The authors have no conflicts to disclose.

Author Contributions

Benjamin W. Zingsem: Conceptualization (supporting); Data curation (equal); Formal analysis (lead); Investigation (equal); Software (lead); Visualization (lead); Writing – original draft (lead); Writing – review & editing (supporting). **Thomas Feggeler:** Data curation (equal); Writing – original draft (supporting). **Detlef Spoddig:** Data curation (supporting);

Investigation (supporting); Methodology (supporting); Writing – original draft (supporting). **Ralf Meckenstock:** Data curation (equal); Methodology (equal); Supervision (equal). **Michael Farle:** Funding acquisition (equal); Resources (equal); Supervision (equal); Writing – review & editing (supporting). **Michael Winklhofer:** Conceptualization (lead); Funding acquisition (equal); Project administration (equal); Resources (equal); Supervision (equal); Writing – review & editing (lead).

DATA AVAILABILITY

The data that support the findings of this study are openly available in Open Science Framework (OSF) at https://osf.io/v7m2n/?view_only=1406e6a38d8241109eef07a3f2908c58, Ref. 28.

REFERENCES

- ¹D. Gandia, L. Marcano, L. Gandarias, D. Villanueva, I. Orue, R. M. Abrudan, S. Valencia, I. Rodrigo, J. Á. García, A. Muela, M. L. Fdez-Gubieda, and J. Alonso, “Tuning the magnetic response of magnetospirillum magneticum by changing the culture medium: A straightforward approach to improve their hyperthermia efficiency,” *ACS Appl. Mater. Interfaces*. **15**, 566–577 (2023).
- ²J. Shen, G. A. Paterson, Y. Wang, J. L. Kirschvink, Y.-X. Pan, and W. Lin, “Renaissance for magnetotactic bacteria in astrobiology,” *ISME J.* **17**, 1526–1534 (2023).
- ³H. Chen, S. D. Zhang, L. Chen, Y. Cai, W. J. Zhang, T. Song, and L.-F. Wu, “Efficient genome editing of *Magnetospirillum magneticum* AMB-1 by CRISPR-Cas9 system for analyzing magnetotactic behavior,” *Front. Microbiol.* **9**, 1569 (2018).
- ⁴D. Faivre and D. Schüler, “Magnetotactic bacteria and magnetosomes,” *Chem. Rev.* **108**, 4875 (2008).
- ⁵A. Körnig, M. Winklhofer, J. Baumgartner, T. P. Gonzalez, P. Fratzl, and D. Faivre, “Magnetite crystal orientation in magnetosome chains,” *Adv. Funct. Mater.* **24**, 3926–3932 (2014).
- ⁶C. Lang, D. Schüler, and D. Faivre, “Synthesis of magnetite nanoparticles for bio- and nanotechnology: Genetic engineering and biomimetics of bacterial magnetosomes,” *Macromol. Biosci.* **7**, 144–151 (2007).
- ⁷D. A. Bazylinski and C. T. Lefevre, “Magnetotactic bacteria from extreme environments,” *Life* **3**, 295–307 (2013).
- ⁸A. Isambert, N. Menguy, E. Larquet, F. Guyot, and J.-P. Valet, “Transmission electron microscopy study of magnetites in a freshwater population of magnetotactic bacteria,” *Am. Miner.* **92**, 621–630 (2007).
- ⁹E. T. Simpson, T. Kasama, M. Pósfai, P. R. Buseck, R. J. Harrison, and R. E. Dunin-Borkowski, “Magnetic induction mapping of magnetite chains in magnetotactic bacteria at room temperature and close to the Verwey transition using electron holography,” *J. Phys.: Conf. Ser.* **17**, 108 (2005).
- ¹⁰R. E. Dunin-Borkowski, M. R. McCartney, M. Pósfai, R. B. Frankel, D. A. Bazylinski, and P. R. Buseck, “Off-axis electron holography of magnetotactic bacteria: Magnetic microstructure of strains MV-1 and MS-1,” *Eur. J. Mineral.* **13**, 671–684 (2001).
- ¹¹R. E. Dunin-Borkowski, M. R. McCartney, R. B. Frankel, D. A. Bazylinski, M. Pósfai, and P. R. Buseck, “Magnetic microstructure of magnetotactic bacteria by electron holography,” *Science* **282**, 1868 (1998).
- ¹²L. Marcano, I. Orue, D. Gandia, L. Gandarias, M. Weigand, R. M. Abrudan, A. Garcia-Prieto, A. Garcia-Arribas, A. Muela, M. L. Fdez-Gubieda, and S. Valencia, “Magnetic anisotropy of individual nanomagnets embedded in biological systems determined by axi-asymmetric X-ray transmission microscopy,” *ACS Nano* **16**, 7398–7408 (2022).
- ¹³D. M. Chevrier, E. Cerdá-Doñate, Y. Park, F. Cacho-Nerin, M. Gomez-Gonzalez, R. Uebe, and D. Faivre, “Synchrotron-based nano-X-ray absorption near-edge structure revealing intracellular heterogeneity of iron species in magnetotactic bacteria,” *Small Sci.* **2**, 2100089 (2021).
- ¹⁴T. Feggeler, R. Meckenstock, D. Spoddig, B. W. Zingsem, H. Ohldag, H. Wende, M. Farle, M. Winklhofer, and K. J. Ollefs, “Spatially resolved GHz magnetization dynamics of a magnetite nano-particle chain inside a magnetotactic bacterium,” *Phys. Rev. Res.* **3**, 033036 (2021).

- ¹⁵X. H. Zhu, A. P. Hitchcock, D. A. Bazylinski, P. Denes, J. Joseph, U. Lins, S. Marchesini, H.-W. Shiu, T. Tyliczszak, and D. A. Shapiro, "Measuring spectroscopy and magnetism of extracted and intracellular magnetosomes using soft X-ray ptychography," *Proc. Natl. Acad. Sci. U. S. A.* **113**, E8219–E8227 (2016).
- ¹⁶K. P. Lam, A. P. Hitchcock, M. Obst, J. R. Lawrence, G. D. W. Swerhone, G. G. Leppard, T. Tyliczszak, C. Karunakaran, J. Wang, K. Kaznatcheev, D. A. Bazylinski, and U. Lins, "Characterizing magnetism of individual magnetosomes by X-ray magnetic circular dichroism in a scanning transmission X-ray microscope," *Chem. Geol.* **270**, 110–116 (2010).
- ¹⁷R. B. Frankel, R. Blakemore, and R. S. Wolfe, "Magnetite in freshwater magnetotactic bacteria," *Science* **203**, 1355–1356 (1979).
- ¹⁸A. Barman, G. Gubbiotti, S. A. Nikitov *et al.*, "The 2021 magnonics roadmap," *J. Phys.: Condens. Matter.* **33**, 413001 (2021).
- ¹⁹B. W. Zingsem, T. Feggeler, A. Terwey, S. Ghaisari, D. Spoddig, D. Faivre, R. Meckenstock, M. Farle, and M. Winklhofer, "Biologically encoded magnonics," *Nat. Commun.* **10**, 4345 (2019).
- ²⁰Q. Wang, T. Brächer, M. Fleischhauer, B. Hillebrands, and P. Pirro, "Stimulated-Raman-adiabatic-passage mechanism in a magnonic environment," *Appl. Phys. Lett.* **118**, 182404 (2021).
- ²¹Q. Wang, B. Heinz, R. Verba, M. Kewenig, P. Pirro, M. Schneider, T. Meyer, B. Lägel, C. Dubs, T. Brächer, and A. V. Chumak, "Spin pinning and spin-wave dispersion in nanoscopic ferromagnetic waveguides," *Phys. Rev. Lett.* **122**, 247202 (2019).
- ²²A. Vansteenkiste, J. Leliaert, M. Dvornik, M. Helsen, F. Garcia-Sanchez, and B. Van Waeyenberge, "The design and verification of MuMax3," *AIP Adv.* **4**, 107133 (2014).
- ²³L. Exl, S. Bance, F. Reichel, T. Schrefl, H. P. Stimming, and N. J. Mauser, "LaBonte's method revisited: An effective steepest descent method for micro-magnetic energy minimization," *J. Appl. Phys.* **115**, 17D118 (2014).
- ²⁴R. Narkowicz, D. Suter, and R. Stonies, "Planar microresonators for EPR experiments," *J. Magn. Reson.* **175**, 275 (2005).
- ²⁵R. Narkowicz, D. Suter, and I. Niemeyer, "Scaling of sensitivity and efficiency in planar microresonators for electron spin resonance," *Rev. Sci. Instrum.* **79**, 084702 (2008).
- ²⁶K. H. Schleifer, D. Schüler, S. Spring, M. Weizenegger, R. Amann, W. Ludwig, and M. Köhler, "The genus *Magnetospirillum* gen. nov. Description of *Magnetospirillum gryphiswaldense* sp. nov. and transfer of *Aquaspirillum magnetotacticum* to *Magnetospirillum magnetotacticum* comb. nov.," *Syst. Appl. Microbiol.* **14**, 379 (1991).
- ²⁷J. Roy, P. R. Teja, S. Sahu, G. A. Basheed, and R. B. Gangineni, "Influence of in-situ annealing temperature upon structural, micro-structural, magnetic damping properties in sputtered Fe₃O₄ thin films," *J. Magn. Magn. Mater.* **585**, 171130 (2023).
- ²⁸See https://osf.io/v7m2n/?view_only=1406e6a38d8241109eef07a3f2908c58 for "4 particle nanomagnonic ensemble derived from AT07_AB12 μ -resonator experiments."